1. Kamsin, M. A. (ed.), In *Pesticide Profiles: Toxicity, Environmental Impact and Fate*, Lewis Publishing, NY, 1997, pp. 147–152.
2. Patil, J. A., Patil, A. J. and Govindwar, S. P., Biochemical effects of various pesticides on sprayers of grape gardens. *Indian J. Clin. Biochem.*, 2003, **18**, 16–22.
3. Ramade, F., *Ecotoxicology*, John Wiley, New York, 1987.
4. Blondell, J., Problems encountered in the design of epidemiologic studies of cancer in pesticide users. *Med. Lav.*, 1990, **81**, 524–529.
5. Moser, V. C., Dose response and time-course of neurobehavioral changes following oral chlorpyrifos in different ages. *Neurotoxicol. Teratol.*, 2000, **22**, 713–723.
6. Whitney, K D., Seidler, F. J. and Slotkin, T. A., Developmental neurotoxicity of chlorpyrifos: Cellular mechanism. *Toxicol. Appl. Pharmacol.*, 1995, **134**, 53–62.
7. Saleha Banu, Dana Devi, Rahman, M. F., Ahuja, Y. R. and Jamil, K., Genotoxic effect of Monocrotophos to sentinel species using comet assay. *Food Chem. Toxicol.*, 2001, **39**, 361–366.
8. Jamil, K., Shaik, A. P., Mahboob, M. and Krishna, D., Effect of organophosphorus and organochlorine pesticides (Monocrotophos, Chlorpyriphos, Dimethoate and Endosulfan) on human lymphocyte cultures *in vitro*. *Drug Chem. Toxicol.*, 2004, **27**, 133–144.
9. Jamil, K., Shaik, A. P. and Jyothi Laxmi, A., Pesticide induced cytogenetic risk assessment in human lymphocyte culture *in vitro*. *Bull. Environ. Contam. Toxicol.*, 2005, **75**, 7–14.
10. Rambabu, N. and Jamil, K., Cytogenetic biomarkers of carbofuran toxicity utilizing human lymphocyte cultures *in vitro*. *Chem. Drug Toxicol.*, 2005, **28**, 359–372.
11. Rambabu, N. and Jamil, K., Evaluation of cytogenetic effects of lambda-cyhalothrin on human lymphocytes. *J. Biochem. Mol. Toxicol.*, 2005, **19**, 304–310.
12. Suman, G., Rambabu, N. and Jamil, K., *In vitro* cytogenetic studies of Cypermethrin on human lymphocytes. *Indian J. Exp. Biol.*, 2006, **44**, 233–239.
13. Moorhead, R. S. *et al.*, Chromosome preparations of leucocytes cultured from human peripheral blood. *Exp. Cell Res.*, 1960, **20**, 613–616.
14. Singh, N. P., Mcvoy, M. T., Tice, R. and Scheneider, L. E., A simple technique for quantitation of low level of DNA damage in individual cells. *Exp. Cell Res.*, 1988, **175**, 184–191.
15. Vojdani, A., Ghoneum, M. and Brautbar, N., Immune alteration associated with exposure to toxic chemicals. *Toxicol. Ind. Health*, 1995, **8**, 239–254.
16. Pearson, S. P. and Stanley, J. R., Quantitative disorders of granulocytes. In *Current Diagnosis 9* (eds Conn, R. B. *et al.*), WB Saunders & Company, Philadelphia, 1997.
17. Broughton, A., Thrasher, J. D. and Madison, R., Chronic health effects and immunological alterations associated with exposure to pesticides. *Comments Toxicol.*, 1990, **4**, 59–71.
18. Zahm, S. H., Ward, M. H. and Blair, A., Pesticides and cancer. *Occup. Med.*, 1997, **12**, 269–289.
19. Dich, J., Zahm, S. H., Hanberg, A. and Adami, H. O., Pesticides and cancer. *Cancer Causes Control*, 1997, **8**, 420–443.
20. Meinert, R. *et al.*, Childhood leukemia and exposure to pesticides: Results of a case-control study in northern Germany. *Eur. J. Cancer A*, 1996, **32**, 1943–1948.
21. Sanderson, W. T. *et al.*, Pesticide prioritization for a brain cancer case – control study. *Environ. Res.*, 1997, **74**, 133–144.
22. Sherman, J. D., Chlorpyrifos (Dursban) exposure and birth defects: a report of 15 incidents, evaluation of cases, theory of action and medical and social aspects. *Eur. J. Oncol.*, 1999, **4**, 53–59.
23. Leiss, J. K. and Savitz, D. A., Home pesticide use and childhood cancer: A case-control study. *Am. J. Public Health*, 1995, **85**, 249–252.
24. Aldridge, J. E., Gibbons, J. A., Flaherty, M. M., Kreider, M. L., Romano, J. A. and Levin, E. D., Heterogeneity of toxicant response: Sources of human variability. *Toxicol. Sci.*, 2003, **76**, 3–20.
25. Persson, B. *et al.*, Some occupational exposures as risk factors for malignant lymphomas. *Cancer*, 1993, **72**, 1773–1778.
26. Costello, R. *et al.*, Philadelphia chromosome-negative chronic myeloid leukaemia: a report of 14 new cases. *Br. J. Haematol.*, 1995, **90**, 346–352.
27. Kantarjian, H., Kurzrock, R. and Talpaz, M., Philadelphia chromosome-negative chronic myelogenous leukemia and chronic myelomonocytic leukemia. *Hematol. Oncol. Clin. North Am.*, 1990, **4**, 389–404.
28. Pasqualetti, P., Casale, R., Colantonio, D. and Collacciani, A., Occupational risk for hematological malignancies. *Am. J. Hematol.*, 1991, **38**, 147–149.
29. Kurzrock, R., Kantarjian, H., Shtalrid, M., Gutterman, J. and Talpaz, M., Philadelphia chromosome-negative chronic myelogenous leukemia without a breakpoint cluster region rearrangement: a chronic myeloid leukemia with a distinct clinical course. *Blood*, 1990, **75**, 445–452.
30. Huret, J. L., Complex translocations, simple variant translocations and Ph-negative cases in chronic myelogenous leukaemia. *Hum. Genet.*, 1990, **85**, 565–568.
31. Martiat, P., Michaux, J. and Rodhain, J., Philadelphia-negative (Ph-) chronic myeloid leukemia (CML): comparison with Ph+ CML and chronic myelomonocytic leukemia. *Blood*, 1991, **78**, 205–211.

ACKNOWLEDGEMENTS. We thank CSIR, New Delhi for the grant of the scheme 21(504)/EMR-II and fellowship to G.P.D. and A.P.S. Thanks are due to Bhagwan Mahavir Medical Research Centre, Hyderabad for providing facilities. We are also grateful to Indo-American Cancer Institute and Research Centre, Hyderabad for help.

Received 10 May 2006; revised accepted 4 September 2006

# Simulation of Antarctic sea ice

**Amitabh Mitra[1] and I. M. L. Das[1,2,*]**

[1]K. Banerjee Centre of Atmospheric and Ocean Studies, Nehru Science Centre, and [2]Department of Physics, University of Allahabad, Allahabad 211 002, India

**Semtner's three-layer sea ice model and Winton's reformulated three-layer sea ice model have been applied to the Antarctic region (where there are chances of sea ice disappearing in the summer leading to open water) for simulating some features of sea ice using the ECMWF re-analysis data. The results of the simulation have been compared with the observation.**

**Keywords:** Antarctica, ECMWF re-analysis, sea ice, Semtner model, Winton model.

IT has been observed over the years that any change in the circulation pattern of the oceans, particularly the deep oceans, results in climatic changes. The characteristics and circulation of 50 to 60% of sub-surface waters in the oceans

*For correspondence. (e-mail: drimldas@yahoo.com)

are determined by what happens at the air–sea interface of the Southern Ocean surrounding Antarctica. It represents about 20% of world ocean surface and the Antarctic sea ice forms an important component of the ocean heat exchange engine. The Antarctic 'sources' of deep water provide one of the major controls on climate. Changes in sea ice cause water mass modification both in the region where ice is formed (or freshwater is removed) and in the region where ice melts (or freshwater is released to the ocean). Further, sea ice is substantially non-uniform in thickness and distribution and does not behave as a passive tracer drifting with the wind or ocean currents. The heat budget of the polar regions is dominated by the presence of sea ice, which reduces the amount of solar radiation absorbed at the earth's surface by a factor of five to eight. This is due to the high albedo of sea ice which ranges between $< 0.5$ for melting bare ice and $> 0.85$ for snow-covered cold ice. In contrast, the ice-free ocean has an albedo of below 0.1. As a result, a reduction in ice extent due to perturbations in the atmospheric heat transfer into the polar regions exposes more of the ocean, which in turn increases the amount of solar heating, further amplifying the ice retreat. Antarctic sea ice extent, ranging between $20 \times 10^6$ km$^2$ (in winter) and $2.5 \times 10^6$ km$^2$ (in summer), is an important component of the global climate system. Its growth and decay have a significant impact on the circulation of the world oceans and on the large-scale oceanic heat and gas transport. Such ice-albedo feedback processes are capable of modulating the global energy balance.

One of the earliest attempts to simulate polar sea ice was by Maykut and Untersteiner[1], which was further simplified by Semtner[2]. Semtner considers a three-layer model for the sea ice, with a single snow layer overlaying two equally thick ice layers with constant heat conductivities. Winton[3] reformulated Semtner's model by considering the upper ice layer to have a variable specific heat resulting from brine pockets and the lower ice layer having a fixed heat capacity. A zero heat capacity snow layer lies above the ice. Heat fluxes at the top and bottom surfaces are used to calculate the changes in ice and snow layer thickness. All prevalent climate models use Semtner's model in one form or the other. Some of the recent climate models such as MIT gcm, have incorporated Winton's reformulation. Both Semtner and Winton have formulated their sea ice models considering only the vertical thermodynamics of sea ice and validated their models for the Arctic region. In the present study, we have applied these models to the Antarctic region where there are chances of sea ice disappearing in the summer and an inter-comparison of the results has been made.

Semtner's three-layer model deals with the thermodynamic part of sea ice considering it to be a static, vertical slab of ice. The thermodynamics used in the model is one-dimensional ($z$) and does not include the horizontal variations of sea ice. Semtner considers one snow layer of thickness $h_s$ lying over two layers of ice of equal thickness ($h_i/2$). The grid points for each layer lie at the centre of the layer. The temperatures in the snow and ice layers are computed using the one-dimensional heat equation:

$$\rho c' \frac{\partial T}{\partial t} = k \frac{\partial^2 T}{\partial z^2}. \quad (1)$$

where $\rho$ is the density of snow or ice, $c'$ the snow or ice heat capacity, $T$ the temperature, $t$ the time, $k$ the snow or ice conductivity and $z$ is the vertical coordinate. Vertical flux balance condition is used to compute changes in thickness of snow and ice layers and changes in the temperature within the layers, at the central grid points.

The driving force of the thermodynamic model is the net heat flux received from the atmosphere in the snow or ice layer, which keeps changing throughout the year. A simple parameterization is used for the energy trapped in brine pockets, which act as reservoirs for heat of fusion. The heat stored in the reservoir is prevented from accumulating more than 30% of the amount needed to melt all the ice. When this maximum is reached, the heat of fusion at the top of the ice is reduced by 30% and heat from the storage reservoir supplies the remainder[2].

For a time step of 8 h, the individual ice layers must remain thicker than 25 cm for the stability of the numerical method and in case they become less thicker, a layer is removed and the temperatures are re-interpolated to the centre of the remaining ice layer. If the total ice thickness drops below 25 cm, the 'three-layer' model switches itself to the 'zero-layer model' using simple mass-budget equations. Similarly, snow temperatures are predicted only for snow thickness above 15 cm. Ice and snow may disappear altogether and again reappear when the sea surface reaches freezing temperature[2].

Winton has reformulated the Semtner's model, but kept the layer structure of the model intact. The thermodynamically active brine pockets are assumed to be concentrated at the upper ice layer. For pure ice, the internal energy per unit mass of ice (J/kg) is

$$E = -L + TC, \quad (2)$$

where $L$ is the latent heat of melting at 0°C, $T$ is the temperature of the ice (in °C) and $C$ is the specific heat of pure ice[4]. Winton[3] used the following expression for the conservation of enthalpy in the upper layer of ice:

$$E_1 = -L\left(1 + \mu \frac{S}{T}\right) + C(T + \mu S), \quad (3)$$

where $S$ is the salinity of the ice and $\mu$ is the ratio of freezing temperature to salinity of brine (with a value of 0.054°C/ppt)[3]. The first term in the expression is the latent heat of the ice fraction while the second term is the enthalpy of ice. Thus the storage of latent heat inside the ice result-

ing from trapping of shortwave radiation by the brine pockets is taken into account. The reformulation improves the model physics by representing the brine content of the upper ice layer with a variable heat capacity and the lower ice layer has a fixed heat capacity. A zero heat capacity snow layer lies above the ice. For the fixed heat capacity lower ice layer the enthalpy is given by

$$E_2 = -L + C(T + \mu S). \quad (4)$$

The surface temperature is determined by balancing the conductive flux to the surface with the upward flux of heat leaving the surface. An excess of conductive flux to the surface is used towards surface melting. At the bottom of the lower ice layer the difference between the oceanic heat flux and the conductive flux of heat upward contributes to melting (or freezing, if negative).

A physically realistic model should accurately represent the heat capacity of sea ice and the energy of melting, which differ from the values of pure ice, especially near 0°C. The difference is mainly due to the brine pockets, which change in size in order to remain in thermal equilibrium with the ice[5]. When there is no snow on the ice, Semtner's model allows ice to store heat up to a certain extent in an internal heat reservoir and this heat is used to keep the upper ice temperature at –0.1°C, unless the heat reservoir is exhausted. Semtner does not make an appropriate correction to the latent heat of melting at the upper ice layer, to account for the internal brine pocket melting. As a result, more energy is applied towards melting at the upper ice layer than is necessary and hence energy is not conserved. However, Winton simulated the brine content of the upper ice rather than parameterizing it, as was done by Semtner to reduce the number of grid points by about one tenth and simplified the use of a complicated differencing scheme needed to allow a long time step[2]. Semtner's model allows storing of heat in a reservoir to account for the heat stored in brine pockets. However, this heat stored needs to be conserved and not parameterized, for correctly estimating the ice growth and decay and the timing of ice thaw and freeze-up[6]. Therefore, in order to make the physics of the Semtner's model more realistic Winton introduced the depth-dependent conductive coupling at the snow–ice interface as well as at the ice interface between the two ice layers. Snow is a poor conductor of heat compared to ice and its presence markedly affects the vertical profile of the ice. As the ice melts, its conductivity decreases and this has to be faithfully represented in a thermodynamic sea-ice model. Semtner had to use an extra temperature grid point $T_o$ at the midpoint of the snow layer and the ice surface temperature $T_i$ is calculated using the flux balance condition between the ice and snow layer as follows:

$$k_i \frac{(T_1 - T_i)}{h_i/4} = k_S \frac{(T_i - T_0)}{h_S/2}, \quad (5)$$

where, $k_i$ is the ice thermal conductivity and $k_s$ is the snow thermal conductivity. But, Winton made effective use of depth-dependent conductive coupling as $k_{1/2}$ at the snow–ice interface and $k_{3/2}$ at the interface between the two ice layers as given below:

$$k_{1/2} \equiv \frac{4k_i k_S}{k_S h_i + 4k_i h_S}, \quad k_{3/2} \equiv \frac{2k_i}{h_i}. \quad (6)$$

This eliminates the use of temperature grid point $T_o$, simplifying the model numeric and reducing the number of initial inputs required for running the model. Further, Semtner used a 10% smaller heat of fusion at the bottom of the ice to compare his model with Maykut and Untersteiner[2], while Winton did not use such approximations. Also, Semtner's model has no provision for snow-to-ice conversion and vice-versa. Hence, Semtner's model may not be able to determine the snow thickness accurately, which is a serious drawback. Winton has made two internal adjustments for this phenomenon, the first converts snow by $\Delta h_s$ below the waterline into upper ice layer by $\Delta h_1$ where

$$\Delta h_s = -\max\left[\left(h_s - \frac{\rho_w - \rho_i}{\rho_s} h_i\right)\frac{\rho_i}{\rho_w}, 0\right],$$

$$\Delta h_1 = \max\left[\left(h_s - \frac{\rho_w - \rho_i}{\rho_s} h_i\right)\frac{\rho_s}{\rho_w}, 0\right], \quad (7)$$

and $\rho_w$, $\rho_i$ and $\rho_s$ are the density of sea water, ice and snow respectively, while $h_i$ and $h_s$ are the ice and snow thickness respectively. The second adjustment is the change in temperature of the upper ice layer due to addition of the zero heat capacity snow to it. This is done on the basis of enthalpy conservation.

As the ice thickness reaches below 25 cm, the three-layer Semtner's model switches itself to the zero-layer model. In Winton's model there is no need of switching to a zero-heat-capacity model as the ice becomes thin, thus reducing the computational time.

Both Semtner[2] and Winton[3] had applied their models in the Arctic region where there is multiyear ice with mean thickness ranging from 3 to 4 m. Therefore, switching of Semtner's three-layer model to zero-layer model is not so evident. In the Antarctic region there are chances of sea ice disappearing in the summer, leading to the formation of open water or leads. About 80% of Antarctic sea ice is composed of thin first-year ice (about 0.5 m in thickness), which disappears in summer.

In the Antarctic region the sea ice thickness variability ranges from 0 to 2 m hence the time stepping in both the models was reduced to 2 h. Consequently, Semtner's 'three-layer' model switches itself to the 'zero-layer' model if the total ice thickness drops below 12.5 cm and the temperature

**Table 1.** Average of 44 years data (1958–2001) from ECMWF re-analysis

| | | Jan. | Feb. | Mar. | Apr. | May | Jun. | Jul. | Aug. | Sep. | Oct. | Nov. | Dec. |
|---|---|---|---|---|---|---|---|---|---|---|---|---|---|
| Incoming shortwave radiation ($F_r$) $Wm^{-2}$ | Mawson | 325.15 | 238.24 | 127.30 | 40.35 | 5.11 | 0.02 | 1.37 | 21.83 | 91.63 | 208.34 | 313.40 | 359.84 |
| | Davis | 335.85 | 225.15 | 110.16 | 30.67 | 2.44 | 0.01 | 0.49 | 15.72 | 80.44 | 195.17 | 313.91 | 376.02 |
| | Casey | 274.03 | 195.02 | 102.88 | 36.64 | 6.41 | 0.78 | 2.64 | 21.64 | 84.38 | 186.95 | 287.16 | 315.68 |
| Incoming longwave radiation ($F_L$) $Wm^{-2}$ | Mawson | 222.79 | 195.23 | 169.88 | 154.18 | 147.65 | 146.26 | 140.74 | 139.31 | 140.27 | 150.72 | 188.11 | 221.31 |
| | Davis | 211.59 | 198.34 | 180.82 | 162.99 | 157.33 | 157.20 | 149.27 | 147.16 | 147.46 | 158.13 | 184.24 | 207.89 |
| | Casey | 259.67 | 248.39 | 235.05 | 216.36 | 207.25 | 207.56 | 202.12 | 197.80 | 193.08 | 204.68 | 227.59 | 251.72 |
| Sensible heat flux ($F_T$) $Wm^{-2}$ | Mawson | 6.12 | 14.53 | 20.91 | 32.77 | 40.18 | 45.29 | 44.09 | 42.40 | 34.13 | 22.12 | 9.61 | 3.17 |
| | Davis | 4.32 | 9.10 | 16.48 | 31.20 | 37.39 | 40.27 | 39.47 | 37.80 | 30.43 | 19.09 | 9.22 | 2.96 |
| | Casey | 0.66 | –1.92 | –9.26 | –11.47 | –2.78 | 7.55 | 11.40 | 9.65 | 5.69 | 1.60 | 1.35 | 0.57 |
| Latent heat flux ($F_l$) $Wm^{-2}$ | Mawson | –16.17 | –11.66 | –9.82 | –4.83 | –3.55 | –3.31 | –2.84 | –3.02 | –3.74 | –6.04 | –13.59 | –20.27 |
| | Davis | –16.65 | –13.35 | –10.03 | –4.41 | –3.29 | –4.04 | –3.97 | –4.49 | –5.01 | –6.91 | –13.02 | –18.34 |
| | Casey | –14.46 | –18.39 | –23.78 | –21.58 | –15.27 | –9.75 | –7.29 | –7.83 | –9.08 | –11.17 | –14.80 | –16.42 |
| Albedo ($\alpha_s$) | Mawson | 0.73 | 0.74 | 0.73 | 0.75 | 0.75 | 0.67 | 0.75 | 0.75 | 0.76 | 0.74 | 0.75 | 0.74 |
| | Davis | 0.62 | 0.6 | 0.63 | 0.7 | 0.72 | 0.71 | 0.7 | 0.73 | 0.74 | 0.74 | 0.71 | 0.65 |
| | Casey | 0.34 | 0.31 | 0.34 | 0.48 | 0.59 | 0.65 | 0.71 | 0.72 | 0.72 | 0.72 | 0.63 | 0.44 |
| Snowfall (cm) | Mawson | 0.71 | 0.62 | 0.48 | 0.46 | 0.49 | 0.49 | 0.53 | 0.6 | 0.47 | 0.43 | 0.75 | 0.79 |
| | Davis | 0.36 | 0.67 | 0.87 | 0.79 | 0.78 | 0.7 | 0.69 | 0.57 | 0.61 | 0.56 | 0.59 | 0.47 |
| | Casey | 0.75 | 0.89 | 1.37 | 1.45 | 1.58 | 1.89 | 1.77 | 1.67 | 1.43 | 1.31 | 1.11 | 0.91 |

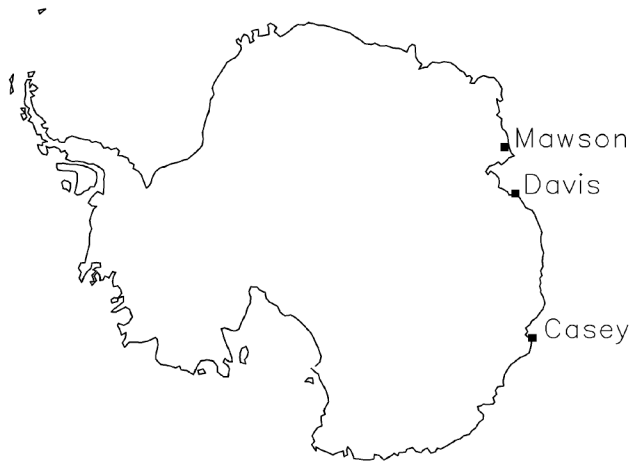


**Figure 1.** Location of Australian Antarctic stations.

grid point $T_o$ at the midpoint of snow layer vanishes if snow thickness drops below 7.5 cm. The ice salinity[5] was kept at 3.2°C/ppt. Both the models were forced with the ECMWF re-analysis data (Table 1), which are monthly means averaged over the period 1958–2001 for the Australian Antarctic stations, Mawson (67°36′S, 62°52′E), Davis (68°34′S, 77°58′E) and Casey (66°16′S, 110°31′E) shown in Figure 1. The albedo $\alpha_s$ of snow is calculated using the relation $S_{net} = S(1 - \alpha_s)$, where $S_{net}$ is the net shortwave radiation and $S$ is the downward shortwave radiation taken from ECMWF. A value[7] of 0.5 was taken for the ice albedo $\alpha_i$. The snowfall data in Table 1 (from ECMWF re-analysis) were converted from 'metres of water equivalent' to centimetres by multiplying it with 100 and then by 10 to allow for a 1 to 10 expansion from water to snow. The snow surface temperature and upper ice temperature were validated from the ECMWF re-analysis data. The ice and snow thickness observations used for validation are those observed at Mawson, Davis and Casey, which are readily available for the years 1982, 1985 and 1979 respectively[8].

Monthly variation of the simulated snow surface temperature, upper ice temperature, ice thickness and snow thickness at the three Australian Antarctic stations obtained from 30-yr integrations of both the models are shown in Figure 2. They represent the simulated monthly values after attaining equilibrium. The monthly variation of snow surface temperature is shown in Figure 2 *a–c*. Both the models overestimate the snow surface temperature at Mawson and Davis except at Casey. Winton's model underestimates the snow surface temperature at Casey during March–June. The snow surface temperatures simulated by both the models are almost the same in the later half of the year at all the three stations.

Variation of the upper ice temperature is shown in Figure 2 *d–f*. Winton's model records a low upper ice temperature at Mawson and Davis throughout the year because a thick layer of simulated ice prevents the oceanic heat flux from the bottom and the high snow albedo in these two regions (see Table 1) obstructs the solar radiation from raising its temperature. The upper ice temperature simulated by Winton's model at Casey is high throughout the year due to comparatively low snow albedo. As the

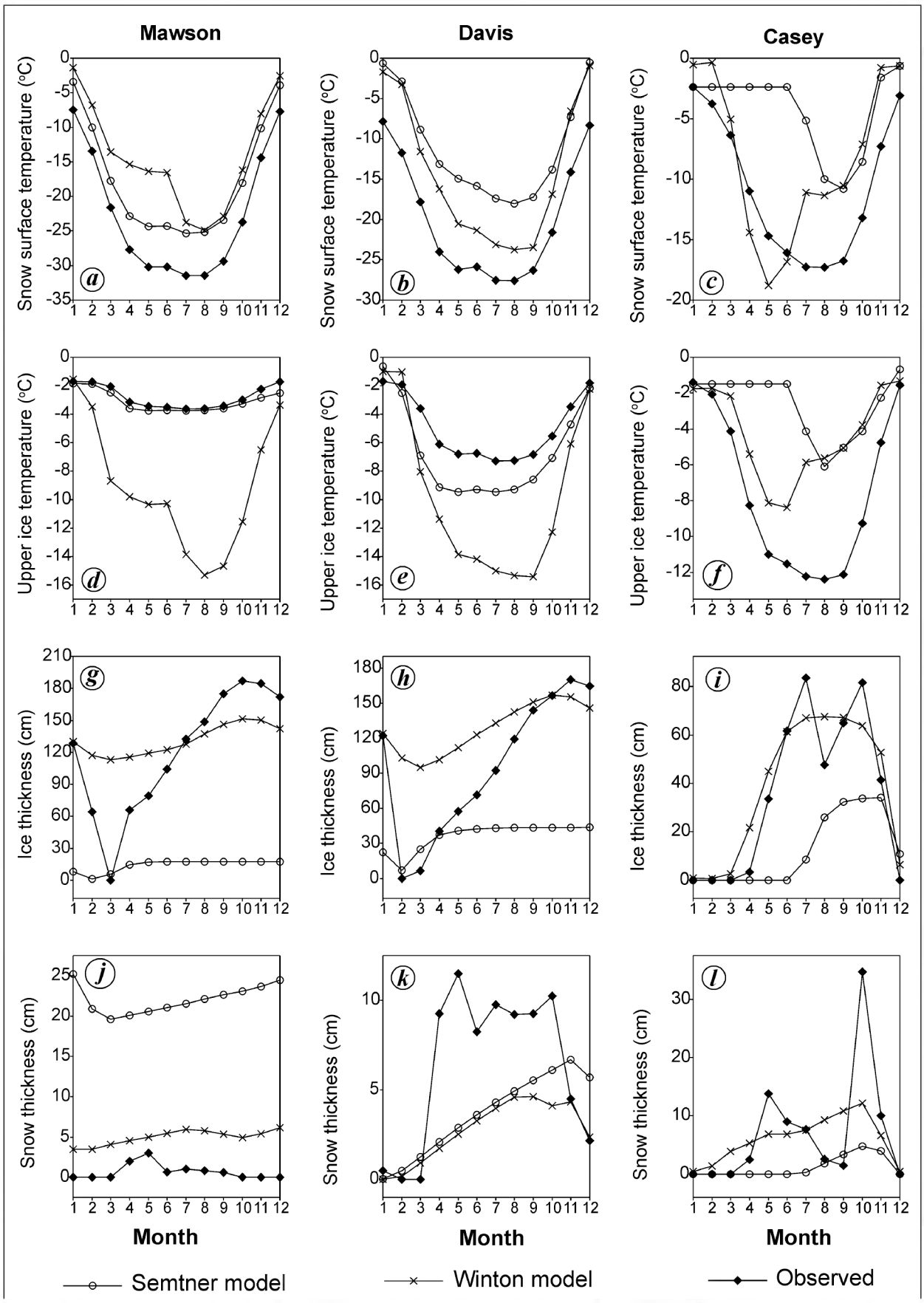


**Figure 2.** Comparison of simulated results with observations.

snow albedo picks up and becomes nearly equal to the values at Mawson and Davis, both the models simulate almost equal upper ice temperature.

The seasonal variation of ice thickness is shown in Figure 2 *g–i*. Semtner's model underestimates the ice thickness considerably at all the stations. This may be due to the fact that there is no provision for conversion of snow to ice or vice versa in Semtner's model, leading to inaccurate determination of snow thickness. The snow layer is less likely to affect the sensitivity of the Arctic sea ice to environmental changes but can affect the response of Antarctic sea ice cover to present or future climatic changes[9]. Also, the high oceanic heat flux in the region contributes to the melting of ice beneath the ice layer. Winton's model overestimates the ice thickness for Davis almost throughout the year, whereas it overestimates the ice thickness for Mawson only for first half of the year. For Casey, there is not much difference between the observed and simulated (from Winton's model) values. As the ice thickness reaches below 12.5 cm, Semtner's three-layer model switches itself to the zero-layer model using simple mass-budget equations. However, the zero-layer thermodynamic model does not allow ice to store heat like the three-layer model and hence it tends to exaggerate the seasonal variability in ice thickness[6].

The monthly change in snow thickness is depicted in Figure 2 *j–l*. Both the models overestimate snow thickness at Mawson, but underestimate it at Davis. The high snow albedo in the Mawson coast reflects back much of the incoming radiative flux, which prevents the snow layer from melting. At Casey, Semtner's model underestimates the snow thickness.

Both the Semtner and the Winton models are able to capture seasonal variability of Antarctic sea ice using only thermodynamics. However, thermodynamics as well as the dynamic processes play a significant role in determining the thickness of sea ice. Ice motion can lead to significant changes in sea ice thickness as well as transport of sea ice. Thus, there is need to investigate sea ice using ice–ocean coupled model that realistically simulates the feedback among the atmosphere, ice and ocean. Antarctic sea ice variability is likely to be controlled by both remote and local processes. Simulating the brine content in the upper ice layer, use of depth-dependent conductive coupling, and the provision of snow-to-ice conversion are advantages in Winton's model.

1. Maykut, G. A. and Untersteiner, N., Some results from a time dependent, thermodynamic model of sea ice. *J. Geophys. Res.*, 1971, **76**, 1550–1575.
2. Semtner, A. J., A model for the thermodynamic growth of sea ice in numerical investigations of climate. *J. Phys. Oceanogr.*, 1976, **6**, 379–389.
3. Winton, M., A reformulated three-layer sea ice model. *J. Atmos. Ocean Technol.*, 2000, **17**, 525–531.
4. Schmidt, G. A., Bitz, C. M., Mikolajewicz, U. and Tremblay, L.-B., Ice–ocean boundary conditions for coupled models. *Ocean Model.*, 2004, **7**, 59–74.
5. Bitz, C. M. and Lipscomb, W. H., An energy-conserving thermodynamic model of sea ice. *J. Geophys. Res.*, 1999, **104**, 15669–15677.
6. Zhang, J. and Rothrock, D., A thickness and enthalpy distribution sea-ice model. *J. Phys. Oceanogr.*, 2001, **31**, 2986–3001.
7. Parkinson, C., Sensitivity studies on a model of the Weddell ice pack. *Antarc. J.*, 1982, **17**, 94–95.
8. Allison, I., Fast ice thickness at Davis, Mawson and Casey. Australian Antarctic Data Centre – CAASM Metadata, 2001; http://aadc-db.aad.gov.au/KeywordSearch/Home.do?Portal=amd_au&MetadataType=0.
9. Fichefet, T. and Maqueda, M. A. M., Modelling the influence of snow accumulation and snow-ice formation on the seasonal cycle of the Antarctic sea-ice cover. *Climate Dyn.*, 1999, **15**, 251–268.

ACKNOWLEDGEMENTS. We thank A. Semtner for providing the code for the zero and three-layer models. We also thank the European Center for Medium-range Weather Forecast for providing data via the website http://www.ecmwf.int. Some of the data used for validation was obtained from the Australian Antarctic Data Centre (IDN Node AMD/AU). This work was supported by the National Centre for Antarctic and Ocean Research, Goa and Department of Ocean Development, Govt of India in the form of a research grant.

Received 25 May 2006; revised accepted 26 August 2006

# Evidences for microbial involvement in the genesis of speleothem carbonates, Borra Caves, Visakhapatnam, India

**Sushmitha Baskar, R. Baskar* and Anubha Kaushik**

Department of Environmental Science and Engineering, Guru Jambheshwar University, Hisar 125 001, India

**Speleothem carbonates are normally considered as inorganic precipitates, but recent work has demonstrated active biological influence in their formations. The present work focuses on the microfabric record and its relation to microbial involvement in the speleothems from Borra Caves, Visakhapatnam. Thin section petrography revealed the presence of lithified structures and micrite, occurring as laminated to clotted with chocolate-brown blebs and identical to microbialites observed in modern and ancient stromatolitic carbonates. SEM observations confirmed the presence of calcified bacteria, micro-rods, and needle calcite. Organic mats (yellow-orange in colour) comprise of mineralized filamentous bacteria, bacterial stalks, cells and sheaths. These microfabric evidences suggest that microorganisms have actively participated in the genesis of speleothem carbonates.**

**Keywords:** Borra Caves, genesis, microbial involvement, speleothem carbonates.

*For correspondence. (e-mail: rbaskargjuhisar@yahoo.com)